Modelling human myoblasts survival upon xenotransplantation into immunodeficient mouse muscle.

Christophe Praud, Karine Vauchez, Pascal Zongo, Jean-Thomas Vilquin

Modelling human myoblasts survival upon xenotransplantation into immunodeficient mouse muscle.

Authors :

Christophe Praud [1], Karine Vauchez [2], Pascal Zongo [1], Jean-Thomas Vilquin[2].

[1] UMR BOA, INRA, Université François Rabelais, 37380 Nouzilly, France.

[2] Sorbonne Université, INSERM, CNRS, Center for Research in Myology, Institute of Myology, F-75013, Paris, France.

Corresponding author : Christophe Praud, PhD, UMR BOA, INRA, Université François Rabelais, 37380 Nouzilly, France.

e-mail : christophe.praud@inra.fr

Phone : + 33 2 47 42 78 45

Fax : + 33 2 47 42 77 78

Keywords :

Human myoblasts, SCID mice, Lamin A/C nuclei, skeletal muscle

Abstract

Cell transplantation has been challenged in several clinical indications of genetic or acquired muscular diseases, but therapeutic success were mitigated. To understand and improve the yields of tissue regeneration, we aimed at modelizing the fate of CD56-positive human myoblasts after transplantation. Using immunodeficient severe combined immunodeficiency (SCID) mice as recipients, we assessed the survival, integration and satellite cell niche occupancy of human myoblasts by a triple immunohistochemical labelling of laminin, dystrophin and human lamin A/C. The counts were integrated into a classical mathematical decline equation. After injection, human cells were essentially located in the endomysium, then they disappeared progressively from D0 to D28. The final number of integrated human nuclei was grossly determined at D2 after injection, suggesting that no more efficient fusion between donor myoblasts and host fibers occurs after the resolution of the local damages created by needle insertion. Almost 1% of implanted human cells occupied a satellite-like cell niche. Our mathematical model validated by histological counting provided a reliable quantitative estimate of human myoblast survival and/or incorporation into SCID muscle fibers. Informations brought by histological labelling and this mathematical model are complementary.

Introduction

Skeletal muscle is composed of syncytial myofibers produced by the extensive fusions of muscle progenitors called myoblasts during embryogenesis, development and growth. Lifelong, this tissue is able to regenerate consecutively to mechanical, chemical or pathological injuries through the mobilisation of a population of quiescent cells known as the satellite cells (*1, 2*). Activation of these satellite cells provides myoblasts, which fuse together or with the neighbouring muscle fibers to secure muscle regeneration. This natural capacity to form syncytial structures allows sharing genetic material brought by exogenous myoblasts, and was considered for the treatment of dystrophic muscles by myoblast transplantation. The first proof of concept brought by Partridge et al. (*3*) was followed by clinical trials in Duchenne muscular dystrophy (DMD) patients (*4*), which reached mitigated success and suggested several issues. Immunological rejection of the donor cells, immediate or delayed apoptosis, necrosis or attrition, long-term differentiation underpinned the necessity to follow the early and late fate of injected cells. The use of immunodeficient animals is now widely accepted in this xenogenic context of transplantation (*5*). Severe combined immunodeficiency (SCID) mice or new immunodeficient models such as $Rag2^{-}/Il2rb^{-}$/DMD mice allowed assessing the survival, fate, myogenicity, transplantation efficiency and potential tumorigenicity of several classes of human skeletal muscle cell populations potentially useable for clinical developments, such as CD133+ (*6*), CD56+ (*7*), Aldehyde dehydrogenase + (*8*) cells, or pluripotent stem cells committed to the myogenic lineage (*9, 10*). These models also allowed exploring strategies to enhance the transplantation efficacies by

quantifying the formation of skeletal muscle fibers of human origin, such as myostatin inhibition (*11, 12*), Wnt3a upregulation (*13*), or pharmacological treatments (*14, 15*). To follow the efficiency of these approaches, researchers assessed human myoblast implantation by quantifying the formation of skeletal muscle fibres of human origin (*6-9, 11, 16*), and/or evaluated the cell survival by human Lamin A/C immunolabelling (*6-9, 12, 13, 16*). Additionnally, the assessment of satellite cell niche occupancy is of particular interest to document the persistence of the regenerative capacity (*6, 7, 9*). Standardized quantification deserves the definition of a dedicated mathematical model to assess human cell survival and fate in animal experiments. In this study, we used experimental data obtained in injecting human CD56-positive myoblasts in a SCID recipient environment to define and validate such a mathematical model. Healthy, undamaged mouse muscles were injected to avoid supplementary variabilities of values linked to the setting of muscle degeneration *in vivo*. We then developed histological procedures to count cells and fibers, in link with their location within the injected muscle. We observed a biphasic curve of cell survival in which a rapid initial loss of human cells reflecting acute cell death is followed by a progressive decline over one month reflecting attrition and the lack of further integration. Human cell number decline was then correlated with a low participation of donor cells in fibre formation over time, without impairing the occupancy of presumptive satellite cell niches. The mathematical model of cell disappearance proposed here is a good predictive model based on a decline equation and also gave us information on human myoblasts ability to incorporate in muscle fibers.

Material and Methods

Animals

Eight weeks-old CB17/SCID mice were kept in standard conditions in our own facilities. All procedures were performed under anesthesia (intraperitoneal injection of 80 mg/kg ketamine, 16 mg/kg xylazine). The animals were sacrificed by injecting a lethal dose of this anesthetic mix. All the procedures were conducted according to the Guide for the care and use of laboratory animals (DHAW publication n° (NIH) 85-23 Office of science and health reports, DRR/NIH, Bethesda MD 20892).

Cell preparation and injection

Muscle biopsies were obtained as surgical wastes and kindly provided by the Association Française contre les Myopathies tissue bank (Myobank, Paris, France) and sampled in agreement with the French bioethics laws (Law n° 94-654 of the 29 July 1994, modified the 22 January 2002). Human cells were prepared using the methodology previously described (*17, 18*). Briefly, the biopsies were minced and digested using collagenase (Liberase, 0.1mg/ml, Roche Diagnotics International Ltd, Germany), then trypsin-EDTA (0.025%, Hyclone, GE Healthcare Inc., France). The cell suspension were filtered through 100 then 40µm cell strainers (BD Biosciences Inc., Bedford, MA, USA) and seeded onto a one-layer cell factory (Nunc, Thermofisher Scientific Inc., France) (*17*). The proliferation medium contained: 80% modified MCDB medium (Hyclone, Thermofisher Scientific Inc., France), 20% defined fetal bovine serum (Hyclone, GE Healthcare Inc., France), antibiotics (Sigma Inc., France), 10 ng/ml of human recombinant basic Fibroblast Growth Factor (R&D Systems, United Kingdom), and 10^{-6}M of dexamethasone (Merck Inc., France). The cultures were settled for 7 days, and then the cells were harvested by trypsinization

and expanded before reaching 80% confluence. At this time, cells were frozen and stored at -80°C. For each experiment, an aliquot was thawed and the cells were proliferated in a cell factory to obtain the number of cells required using the proliferation medium mentioned above. Cells were detached using trypsin-EDTA and suspended in MCDB medium with 0.5% Bovine serum albumin (Sigma Inc., France) for the injection. The same amount of living cells was delivered in each mouse. A portion of the harvested cells underwent a specific drastic treatment to be used as a negative control: they were submitted to three rapid freezing-thawing cycles, without cryopreservant. This portion is then considered as a “dead cell fraction”.

Cell phenotype and viability

The CD56 phenotype and the cell viability (evaluated by propidium iodide exclusion) were determined by cytofluorimetry (FACS Calibur and Cellquest software, BD Biosciences Inc., San Jose, CA, USA). Human myoblasts were characterized by their CD56 expression, which reached 90% of total cells within two passages as described previously (*17, 19, 20*). After completion of the cell injection procedure, 7.8% of the cells (remaining in the syringe and needle) stained positive for propidium iodide. These results underlined the preservation of the cell phenotype and a low cell death during the cell injection procedure.

Experimental design

Cell injections were performed in the *Tibialis anterior* muscle (TA) of anesthetised animals (n=6 for each time-point). A small incision was done to visualise the muscle nearby the knee insertion. The needle (Gauge 26S) of a 10 µl Hamilton syringe filled with the cell suspension ($9x10^5$ cells per muscle) was inserted in the proximal part

and up to the distal tendon (Figure 1), then pulled out while the cell suspension was injected. At the end of the experiment, remaining cells not injected were used to quantify the CD56 on cytometry analysis. All the injections were done with the same cell suspension. Following injection, muscles were sampled at days D1, D2, D3, D4, D5, D7, D14 and D28 (Figure 1). A specific *ex vivo* experimental protocol was used to study the fate of cells at time 0, allowing minimally manipulating the muscles after cell injection. In parallel to the classical cell transplantation procedure *in vivo*, some animals were sacrificed and immediatly thereafter their TA were collected, injected *ex vivo* with the cell suspension, and frozen within 15 minutes. Muscles injected with the dead cell fraction were sampled at D1.

Sampling, histology and immunohistochemistry

The TA muscles were snap-frozen in nitrogen-cooled isopentane. Five µm thick serial cryostat cross-sections were performed and collected. They were ranked on consecutive slides to obtain series spaced by 200 µm, from the knee insertion to the distal tendon of the TA (Figure 1).

Morphology of injected muscles was analyzed on slides stained with hematoxylin-eosin. Immunohistochemical analysis was performed using (i) co-immunolabelling of human Cox2 and human lamin A/C to quantify the number of fibers expressing human antigens and (ii) co-immunolabelling of human lamin A/C, human and murine dystrophin, and human and murine laminin to follow the fate of human cells. Antibodies were diluted in goat serum 1% in phosphate buffer saline (PBS, Sigma Inc., France). First, 10% goat serum in PBS was applied on the sections for nonspecific binding blocking. Primary antibodies were a rabbit anti-human Cox2 polyclonal antibody (kind gift of Dr. Anne Lombes, 1/1000 (*21*)), a mouse monoclonal antibody directed against the C-terminus of human dystrophin (NCL-DYS2, with

murine dystrophin crossreactivity, Leica-Biosystems Inc., France, 1/20), a mouse anti-human lamin A/C antibody (Vector Laboratories, United Kingdom, 1/100) and a rabbit anti-rat laminin antibody (with human and murine laminin crossreactivity, Agilent Technologies Inc., Santa Clara, CA, USA, 1/700). Labelling was visualized by using Alexa 350-conjugated goat anti-mouse (Thermofisher Scientific Inc., France, 1/1000), FITC-conjugated goat anti-rabbit (Sigma Inc., France, 1/2000), and Cy5-conjugated goat anti-mouse (IgG2b isotype, SouthernBiotech, Birmingham, AL, USA, 1/1000) antibodies. Slides were mounted in Mowiol or Mowiol-DAPI.

Imaging

Fluorescence imaging on tissue was done using a Zeiss Axioplan 2 Microscope and a Camera Photometric CoolSnap fx (Roper Scientific Inc., Tucson, AZ, USA) controlled by the Metavue 6.2r6 software.

Cell survival analysis

The first cross-section done on each TA muscles was referred as the position 0 µm. As described earlier, on a given slide, consecutive cryosections were separated by 200 µm. Following immunohistochemical labelling, the sections were observed with microscope from the proximal to the distal part of TA. The first and the last sections containing nuclei expressing human lamin A/C were noted, together with their precise localization within the muscles. In addition, six more sections containing human lamin A/C positive nuclei were selected at regular intervals, in which lamin A/C-positive nuclei were counted. Each point was drawn on a graph linking the number of human nuclei to the position of the section in TA muscle in µm. A regression analysis was

done on this curve or in relevant portions of the curve. We hypothesized that the regression curves reflected the distribution of the number of human nuclei all along the muscle length. Regression curve equations were integrated over the entire muscle length (Figure 1). The result obtained was divided by the human nucleus mean size (9 µm, measured and averaged on more than 1000 nuclei, data not shown), providing the total number of human nuclei. The yield of integration into muscle fibers was studied by counting fibers containing at least one human nucleus.

Intramuscular location of the transplanted cells

Using triple labelling of dystrophin, laminin and lamin A/C, two indexes were defined to assess human cell behavior in the SCID TA: the externalization index was defined as the percentage of human nuclei outside the basal lamina, and the internalization index was defined as the percentage of human nuclei underneath the basal lamina. Human nuclei were considered at the satellite-like cell position when they were positioned underneath the basal lamina detected by the laminin expression and on the outside of the sarcolemma revealed by dystrophin immunodetection.

The time effect on the cell disappearance was evaluated by a two-way ANOVA and the three populations of nuclei were compared using a Student's T test ($p<0.05$, Statview 5.0 Software, SAS Institute Inc., Cary, NC, USA).

N(t) is the human cell nuclei number at time t. This number was modelized by the following ordinary differential equation:

$$\frac{dN(t)}{dt} = A + (\lambda - \mu) \cdot N(t)$$
$$N(o) = No > 0$$

Where: A is the differenciation recruitment in the cell population; λ is the proliferation rate; μ is the death rate; N(o) is the initial human cell number at time equal to zero. These values were determined using the experimental data.

Results

Cell survival analysis

Human nuclei were counted on tissue sections after sacrifice of the animals from a few minutes to 28 days after the injection. The number of human nuclei counted after the *ex vivo* injection (D0) was indexed as the 100% cell survival, because it was considered the maximal number of cells remaining in the tissue after injection (Figure 2). As a negative control, we injected the dead cell fraction obtained after 3 cycles of freezing-thawing. In this case, a few cells were still expressing human Lamin A/C (about 0.3% or less than 1500 cells) and still survived the drastic repeated freezing and thawing sequence. When living cells were injected, rare mitotic events were observed at D1 in the injection area on hematoxylin-eosin stained sections (one event for 6 muscles; not shown). The number of human nuclei progressively decreased with time from a percentage of 88 +/- 16.63% of the original cell population still remaining in the tissue at D1 to the disappearance of 93.96 +/- 2.09% of the injected cells at D28 ($p<0.0001$) (Figure 2).

Histological appraisal of cell fate

Immunohistofluorescence analysis showed clusters of human nuclei into injected muscles. Co-immunolabelling of human Cox2 and human lamin A/C allowed counting a maximum of 40 myofibres expressing human Cox2 on a single section (Figure 3C). To localise more precisely human nuclei, we performed a triple labelling of laminin, dystrophin, and human-specific lamin A/C. Thus we could discriminate internalized

cells from externalized cells on the basis of their position according to basement membranes, and the integration of some cells into satellite-like cell position.

At D2, 95.96 +/- 0.87% of cells were present as interstitial clusters. We observed a low proportion of human nuclei within the fibers compared to those observed in the interstitial space. Most fibers containing human cells were undergoing necrosis (94,8% +/- 1%), as they presented a discontinuous laminin labelling and/or an absence of dystrophin (Figure 3A).

At D7, 89.72 +/- 1.67% of human nuclei were also present in the intersititial spaces while some nuclei were observed in regenerating fibers (Figure 3B, Figure 4A, Table 1).

At D14 and D28 the total number of human nuclei was greatly reduced concomitantly to a relative change in proportion between the two compartments (Figure 3C-3D). We first observed an increase of internalization index with time (p=0.002) mainly due to the appearance of human nuclei in muscle fibres from D2. The percentage of internalized nuclei increased mainly from D0 to D2, then decreased between D7 and D28 (Figure 4A). In parallel, we observed a progressive decrease in the externalization index (p=0.0031) (Figure 4A). This underlined a rapid loss of external nuclei within the first two days, then a more progressive, slow loss of external nuclei with time down to 57.33 /- 13.98% at D28.

The triple labelling allowed detecting some human nuclei (Figure 3G) in a putative satellite cell position (Figure 3H), i.e. beneath the sarcolemma detected by dystrophin staining (Figure 3F) and basal lamina detected by laminin staining (Figure 3E). Human nuclei in a satellite-like cell position were never observed between D0 and D7 and first observed at D14 (0.27 +/- 0.18%). At D28, an increase of their proportion

was noted up to 0.96 +/- 0.47% representing 30-50 putative satellite cells in the entire muscle (data not shown).

Modelization of cell behavior

Our mouse model did not undergo muscle fiber regeneration, except for the muscle fibers damaged by the injection. We observed only extremely rare figures of mitosis. The ordinary differential equation describing a decline was then simplified by approximating the human cell proliferation to zero. The new resulting equation becomes:

$$\frac{dN(t)}{dt} = A - \mu \cdot N(t)$$
$$N(o) = No > 0$$

By solving the ordinary differential equation, we obtained explicitly:

$$N(t) = \frac{A}{\mu} \cdot (1 - e^{-\mu t}) + No \cdot e^{-\mu t}$$

Taking into account the experimental results, we obtained μ at 0.18 and A at 7000. N(t) tends to 38889 cells.

A modelization curve is presented in the figure 4B. Maximal predicted cell loss (at 1 month) was of 93.37% of injected cells and was very close to that observed experimentally (93.96%).

Discussion

Muscle cell therapy has been developed to improve skeletal muscle function in several human diseases. Major targets of this approach are chronic genetic diseases such as muscular dystrophies (Duchenne, facio-scapulo-humeral or oculo-pharyngeal muscular dystrophies (*22*)) or acquired diseases such as urethral incontinence (*23, 24*). Causes of these disorders are usually a progressive or acute defect of the regeneration process. Although some clinical results have been encouraging, most of these approaches did not become therapeutic solutions and a better knowledge of muscle cell biology and integration is mandated to improve efficacy.

Strengths and limitations of the mouse model

Our present goal was to modelize both the cell survival and the cell integration of human CD56-positive myoblasts into skeletal muscle. To validate our mathematical model, we acquired experimental data by injecting human cells at a single longitudinal site into the healthy (non-injured) TA muscles of SCID mice. This protocol avoids both an important damaging of the muscle tissue, and the dispersal of cells at too many sites. Therefore, it limits variability and allows standardization. On the other hand, the regenerative potential in these conditions is presumably very low due to the absence of a stimulating, regenerative environment, which is an extrinsic limitation of the model.

An intrinsic limitation of this xenotransplantation model is represented by interspecies molecular differences between human grafted cells and the murine recipient tissue, which may limit the efficacy of cell recognition and fusion. Indeed, several proteins are involved in cellular interactions and close adhesions, such as ADAM12, CD36, integrin alpha3, integrin alpha9, integrin beta1, Jamb, Jamc, Kirrel, M-Cadherin,

NCAM, N-Cadherin, neogenin, nephrin (*25-28*). While these structures are extremely conserved from Homo Sapiens to Pan Troglodytes (mean, 99%) or Macacca Mulatta (mean, 97%), they may show important evolutions in Mus Musculus (mean identity with Homo sapiens is 89%). Of note the murine Jamb and Jamc proteins involved in cell recognition and close adhesion through heterophilic interactions show only 80% and 87% identity with their human homolog, which may hamper a perfect fitting between human and murine actors of cell fusion. These observations would deserve further studies of efficacy of direct protein-protein interactions. Therefore, both extrinsic and intrinsic factors may limit the regenerative processes that usually culminate in cell fusion and fiber accretion.

Robustness of the analyis

In spite of these limitations, to characterize our experimental model, we developed a cell count methodology based on the co-immunolocalisation of human lamin A/C nuclei and murine markers of the sarcolemma (dystrophin) and of the basal lamina (laminin). This direct detection method allowed us to quantify both the human cell survival and cell fate. To reflect more closely the reality, we quantified human nuclei throughout length of the muscles analysed. As a cell count in the negative control, we used a preparation of cells that was presumably killed by repeated freezing-thawing cycles without cryoprotectant (*29*). Surprisingly, approximately 0.3% of the cells (1500) apparently survived these drastic treatments and could be detected 24 hours after injection. Although unexpected, this low percentage of survival validated the methodology of measuring the presence and viability of the cells. Such a phenomenon has been described previously using a methodology based on radionucleotide counting (*29*), and it was hypothesized that the inserted radionucleotide was not immediately cleared by macrophages after killing the cells by

repeated freezing and thawing. In our study, the nuclear lamin protein integrity was assessed as it labelled the perinuclear membrane, however it is still possible that all cellular debris were not removed by inflammatory cells at the time of histological assessment. Whether the cells that we counted were still viable, or should be considered as false positive, their number was very low when compared to the number of injected cells and we considered that this count validated indeed the sensitivity of our counting method.

In this study, we used the experimental data described above to propose a mathematical model assessing the cell disappearance. The several and consecutive experimental data harvested allowed validating the proposed model. We discarded the potential immediate proliferation of the injected cells as this parameter in our model is negligible compared to the death rate. Indeed we only observed rare mitotic events at D1 in the injection area. This parameter, when known or calculated, may still be introduced in the equation to improve the predictivity. As described in the results section, maximal predicted cell loss was very close to that observed experimentally that makes this mathematical model a good predictive one. Finally this model measured also the ability of human myoblasts to incorporate muscle fibers as N(t) tends to the number of human nuclei incorporated in SCID mice skeletal muscle fibers. But it cannot modelize the number of skeletal muscle fibers repopulated by human nuclei.

Kinetics of cell survival

The cell survival study showed a progressive disappearance of CD56-positive myoblasts, which was slower than the acute cell death obtained by injecting human cells into normal immunocompetent mice in a xenogenic context (*21*). This is due to the SCID immunodeficient environment, which avoids the short- and long-term

rejection of the grafted cells. However, we observed a 94% disappearance of injected cells at 1 month. This cell disappearance was associated with a great limitation in cell integration into myofibers as demonstrated by the low number of human Cox2-expressing fibers observed (less than 1% of total fibers).

The disappearance of externalized human nuclei paralleled that of total human nuclei. It suggests the loss of differentiation or fusion capacity of injected cells as observed in previous studies (*30*). Human cells remain during a few weeks in the endomysium in which time window they could be solicited to improve regeneration. However, cells that did not participate to fibre formation and regeneration were progressively committed to disappearance. The number of human nuclei integrated within the first two days was indeed maintained at D7, D14 and D28. Then once integrated in regenerative fibers, these nuclei were maintained. The unavailability to fuse with uninjured myofibres could be related to the factors presented above (1) the molecular differences between human and murine species and lack of appropriate recognition or interaction of molecules involved in cell-cell fusion, (2) the low regenerative context and the absence of expression of adhesion molecules at the surface of recipient myofibers or (3) a decrease of the regenerative potential of myoblasts due to the high density of cells at the injection site. This last hypothesis may be conforted by the observation by Skuk et al. (*31*) that cell death was proportionally linked to the number of cells injected due to the local lack of oxygen and nutrients.

<u>Do human myoblasts contribute to satellite cell niche repletion in mouse?</u>

Although the integration of injected cells was very low, we observed some human cells in satellite-like position in the recipient SCID muscles at D14 and D28. The proportion of cells expressing human lamin A/C at this specific location reached

0.96% of the total human nuclei counted at D28, suggesting the capacity of the injected myoblasts to integrate or constitute *de novo* a satellite cell niche. On one hand, some injected myoblasts may have kept some stemness attributes, at least the capacity to form a stock of repopulating cells, and maybe the capacity to self-renew, despite the species barrier encoutered in our model. The long-term persistence of myoblasts within non-muscle tissue (myocardium) has been documented previously (*32*). On the other hand, the true capacities of these satellite-like cells are unknown. The topography may not reflect the biology. The mechanism by which these human nuclei occupy a satellite-like cell niche in the murine tissue is unclear. The regeneration observed in our model was consecutive to a local, segmental necrosis and focal disruption of basal lamina due to needle penetration, allowing some cells to be injected underneath basal lamina. After necrosis, basal lamina was restored around the original structure (as observed in figure 3 at D7). It is conceivable that, at this moment, some internalized human nuclei may be trapped between the myofiber sarcolemma and basal lamina deposition before any cell-cell fusion. By consequence the trapped cells seem to occupy a satellite-like cell position. Nevertheless, the formation of Pax7-positive cells occupying a murine satellite cell niche after intramuscular transplantation in SCID mice has been also previously described (*7*).

The number of human nuclei incorporated in fibers seemed to be determined at D2 after the injection and represent less than 3% of the cell number injected. And, the injected cells occupying a satellite-like position did not appear before D14 and represent less than 1% of the internalized nuclei. Such a paucity makes difficult the modelization of the human nuclei internalization and of satellite cell positonning.

Conclusion

Our experimental model underlines the low integration rate of the grafted myoblasts in an healthy muscle in the context of xenogenic transplantation (human into mouse) and in the absence of extensive muscle fibre regeneration. The use of xenotransplantation of human myoblasts into immunodeficient mice is routinely used for different transplantation studies, and this method is the easiest to study their behavior after grafting, because it documents both survival and distribution of cells. The experimental model used in this study allowed us to validate a predictive mathematical model of the cell survival that could be used in further studies to estimate and compare the cell survival of different types of myogenic progenitors in a xenogenic transplantation context and their ability to fuse with SCID mice muscle fibers.

Acknowledgements

We wish to thank the AFM (Association Française contre les myopathies) and Association Institut de Myologie for financial support. This study was supported in part by the European Community (Key action 1.2.4-3 Integrated Project Genostem, contract No. 503161). We wish to express special thanks to Stéphane Vasseur and Maud Chapart for the providing of human tissues through the AFM Tissue Bank for Research (Myobank). CP also addresses special thanks to Pr. Michel Fardeau, Mrs. Huguette Collin, Martine Chevallay, Danielle Chateau and Andrée Rouche who learned him everything in muscle histology and morphometry. We pay tribute to Huguette Collin through this article.

References

1. Mauro A. Satellite cell of skeletal muscle fibers. J Biophys Biochem Cytol 1961; 9: 493.
2. Schultz E, Jaryszak DL, Valliere CR. Response of satellite cells to focal skeletal muscle injury. Muscle Nerve 1985; 8 (3): 217.
3. Partridge TA, Grounds M, Sloper JC. Evidence of fusion between host and donor myoblasts in skeletal muscle grafts. Nature 1978; 273 (5660): 306.
4. Gussoni E, Pavlath GK, Lanctot AM, et al. Normal dystrophin transcripts detected in Duchenne muscular dystrophy patients after myoblast transplantation. Nature 1992; 356 (6368): 435.
5. Huard J, Verreault S, Roy R, Tremblay M, Tremblay JP. High efficiency of muscle regeneration after human myoblast clone transplantation in SCID mice. J Clin Invest 1994; 93 (2): 586.
6. Meng J, Chun S, Asfahani R, Lochmuller H, Muntoni F, Morgan J. Human skeletal muscle-derived CD133(+) cells form functional satellite cells after intramuscular transplantation in immunodeficient host mice. Mol Ther 2014; 22 (5): 1008.
7. Skuk D, Paradis M, Goulet M, Chapdelaine P, Rothstein DM, Tremblay JP. Intramuscular transplantation of human postnatal myoblasts generates functional donor-derived satellite cells. Mol Ther 2010; 18 (9): 1689.
8. Vauchez K, Marolleau JP, Schmid M, et al. Aldehyde dehydrogenase activity identifies a population of human skeletal muscle cells with high myogenic capacities. Mol Ther 2009; 17 (11): 1948.
9. Darabi R, Arpke RW, Irion S, et al. Human ES- and iPS-derived myogenic progenitors restore DYSTROPHIN and improve contractility upon transplantation in dystrophic mice. Cell Stem Cell 2012; 10 (5): 610.
10. Chal J, Oginuma M, Al Tanoury Z, et al. Differentiation of pluripotent stem cells to muscle fiber to model Duchenne muscular dystrophy. Nat Biotechnol 2015; 33 (9): 962.
11. Fakhfakh R, Lee SJ, Tremblay JP. Administration of a soluble activin type IIB receptor promotes the transplantation of human myoblasts in dystrophic mice. Cell Transplant 2012; 21 (7): 1419.
12. Fakhfakh R, Michaud A, Tremblay JP. Blocking the myostatin signal with a dominant negative receptor improves the success of human myoblast transplantation in dystrophic mice. Mol Ther 2010; 19 (1): 204.
13. Hwang Y, Suk S, Shih YR, et al. WNT3A promotes myogenesis of human embryonic stem cells and enhances in vivo engraftment. Sci Rep 2014; 4: 5916.
14. Fakhfakh R, Lamarre Y, Skuk D, Tremblay JP. Losartan enhances the success of myoblast transplantation. Cell Transplant 2012; 21 (1): 139.
15. Gerard C, Dufour C, Goudenege S, Skuk D, Tremblay JP. AG490 improves the survival of human myoblasts in vitro and in vivo. Cell Transplant 2012; 21 (12): 2665.
16. Vallese D, Negroni E, Duguez S, et al. The Rag2(-)Il2rb(-)Dmd(-) mouse: a novel dystrophic and immunodeficient model to assess innovating therapeutic strategies for muscular dystrophies. Mol Ther 2013; 21 (10): 1950.
17. Vilquin JT, Marolleau JP, Sacconi S, et al. Normal growth and regenerating ability of myoblasts from unaffected muscles of facioscapulohumeral muscular dystrophy patients. Gene Ther 2005; 12 (22): 1651.

18. Menasche P, Hagege AA, Vilquin JT, et al. Autologous skeletal myoblast transplantation for severe postinfarction left ventricular dysfunction. J Am Coll Cardiol 2003; 41 (7): 1078.
19. Hagege AA, Marolleau JP, Vilquin JT, et al. Skeletal myoblast transplantation in ischemic heart failure: long-term follow-up of the first phase I cohort of patients. Circulation 2006; 114 (1 Suppl): I108.
20. Le Ricousse-Roussanne S, Larghero J, Zini JM, et al. Ex vivo generation of mature and functional human smooth muscle cells differentiated from skeletal myoblasts. Exp Cell Res 2007; 313 (7): 1337.
21. Praud C, Vauchez K, Lombes A, Fiszman MY, Vilquin JT. Myoblast xenotransplantation as a tool to evaluate the appropriateness of nanoparticular versus cellular trackers. Cell Transplant 2008; 17 (9): 1035.
22. Briggs D, Morgan JE. Recent progress in satellite cell/myoblast engraftment -- relevance for therapy. FEBS J 2013; 280 (17): 4281.
23. Huard J, Yokoyama T, Pruchnic R, et al. Muscle-derived cell-mediated ex vivo gene therapy for urological dysfunction. Gene Ther 2002; 9 (23): 1617.
24. Praud C, Sebe P, Bierinx AS, Sebille A. Improvement of urethral sphincter deficiency in female rats following autologous skeletal muscle myoblasts grafting. Cell Transplant 2007; 16 (7): 741.
25. Hindi SM, Tajrishi MM, Kumar A. Signaling mechanisms in mammalian myoblast fusion. Sci Signal 2013; 6 (272): re2.
26. Kim JH, Jin P, Duan R, Chen EH. Mechanisms of myoblast fusion during muscle development. Curr Opin Genet Dev 2015; 32: 162.
27. Krauss RS. Regulation of promyogenic signal transduction by cell-cell contact and adhesion. Exp Cell Res 2010; 316 (18): 3042.
28. Pavlath GK. Spatial and functional restriction of regulatory molecules during mammalian myoblast fusion. Exp Cell Res 2010; 316 (18): 3067.
29. Skuk D, Caron NJ, Goulet M, Roy B, Tremblay JP. Resetting the problem of cell death following muscle-derived cell transplantation: detection, dynamics and mechanisms. J Neuropathol Exp Neurol 2003; 62 (9): 951.
30. Praud C, Montarras D, Pinset C, Sebille A. Dose effect relationship between the number of normal progenitor muscle cells grafted in mdx mouse skeletal striated muscle and the number of dystrophin-positive fibres. Neurosci Lett 2003; 352 (1): 70.
31. Skuk D, Paradis M, Goulet M, Tremblay JP. Ischemic central necrosis in pockets of transplanted myoblasts in nonhuman primates: implications for cell-transplantation strategies. Transplantation 2007; 84 (10): 1307.
32. Ghostine S, Carrion C, Souza LC, et al. Long-term efficacy of myoblast transplantation on regional structure and function after myocardial infarction. Circulation 2002; 106 (12 Suppl 1): I131.

Table 1: Quantification of the CD56-positive human myoblast behavior in SCID TA muscle from D0 to D28 after their injection.

Time	**D1 DC**	**D0**	**D2**	**D7**	**D14**	**D28**
Externalization index	100 (0)	100 (0)	95.96 (0.87)	89.72 (1.67)	78.42 (8.01)	57.33 (13.98)
Internalization index	0	0	4.04 (0.87)	10.34 (1.67)	21.58 (8.01)	42.67 (13.98)
% cell survival	0.27 (0.13)	100 (10.65)	50.14 (13.75)	34.49 (6.89)	17.48 (6.28)	6.04 (2.09)
% nuclei at satellite cell position	0	0	0	0	0.27 (0.18)	0.96 (0.47)

D1DC describes the control muscles injected with dead cell fraction. D0 corresponds to the muscles grafted *ex vivo* and immediatly frozen, which serve to observe the location of the cells immediatly after the injection and to establish the 100% of the grafted cells. Externalization and internalization indexes were provided as mean percentages (S.E.M.) compared to the total human lamin A/C positive nuclei in the respective muscles. The mean percentage of human nuclei located in a satellite-like cell position is also presented.

Figure legends:

Figure 1: Experimental design and procedures.

This figure summarizes all the experimental procedures performed in this study. The experimental design was represented by the timeline from injection time (INJ) at time 0 to all the sampling days (S. Day axis) from D0 to D28. The injection and histological procedures were schematized to illustrate and support the textual descriptions. The total human lamin A/C positive nuclei calculation was illustrated by the graph linking the number of human nuclei to the position of the section in TA muscle in µm done for each muscle and the mathematical formula. Number of human nuclei in each muscle was calculated by integration of linear functions (obtained by linear regression on relevant sections in the curve) and divided by the mean nucleus size.

Figure 2: Survival of human cells grafted in SCID mouse muscles.

Follow-up of human nuclei from D0 to D28. The human lamin A/C-positive nuclei were counted on eight serial sections, using six muscles per time point. Bar graph shows the mean and standard deviation. The number of human nuclei statistically decreased with time ($p<0.0001$).

Figure 3: Human myoblast fate in SCID mouse TA muscle (dystrophin in blue, human lamin A/C in red and laminin in green, co-immunolabellings).

A- At D2, grafted cells were present in clusters, some nuclei being internalized in necrotic myofibres demonstrating a dystrophin negative pattern and/or a discontinuous laminin labelling (white arrow). **B**- At D7, the injected cells were still gathered in clusters and internalized nuclei were observed in regenerating myofibres (white arrow). **C**- At D14, human mitochondria transferred upon fusion of human cells

exhibit the Cox-positive staining (green) in some muscle fibers, which were also frequently containing human nuclei. The human-derived muscle fibers were not numerous and their absolute number did not dramatically evolve from D2 to D28. **D**- At D28, human internalized nuclei were observed in myofibres (asterisk). **E to H-** Human lamin A/C-positive nuclei (**G**) were observed at several positions in the injected muscle, some being in interstitial place (thick arrow), some being trapped between the laminin sheath and the dystrophin edging (therefore, in a satellite-like cell position, asterisk), some being integrated within muscle fibers below their dystrophin edging (fine arrow). **E** is the laminin staining, **F** the dystrophin staining, **G** the lamin A/C staining and **H** the merge image.

Scale bar at the bottom left: A to C- 100 µm; D- 65 µm; E to H-20 µm.

Figure 4: Quantification of human cell survival and modelization of cell survival.

A- Follow-up of human nuclei from D0 to D28 according to their localization: in (internalized) and out (externalized) of the muscle fibre. Different fonts were used to distinguish each nucleus localization. **B**- After modelization of cell survival using the experimental points, the mathematical model shows a progressive cell disappearance of human nuclei.

572 Figure 1

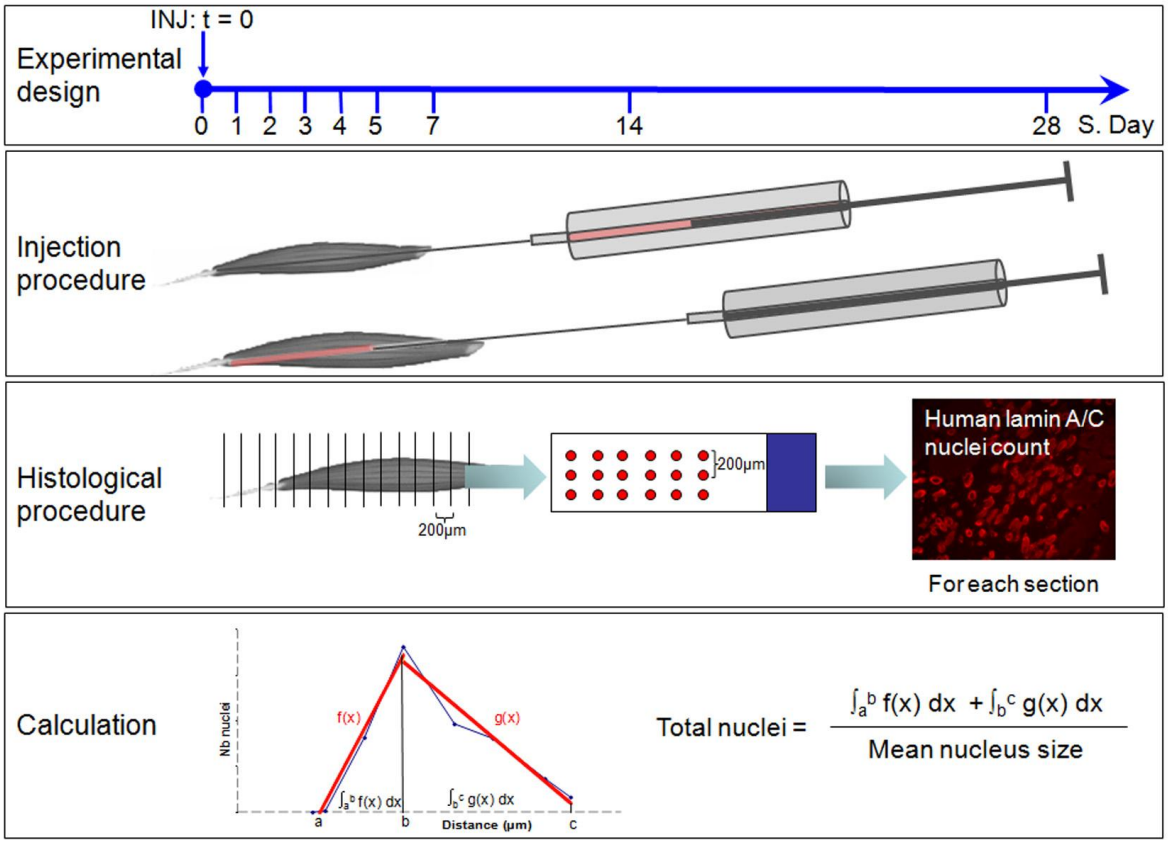

573

574

575 Figure 2

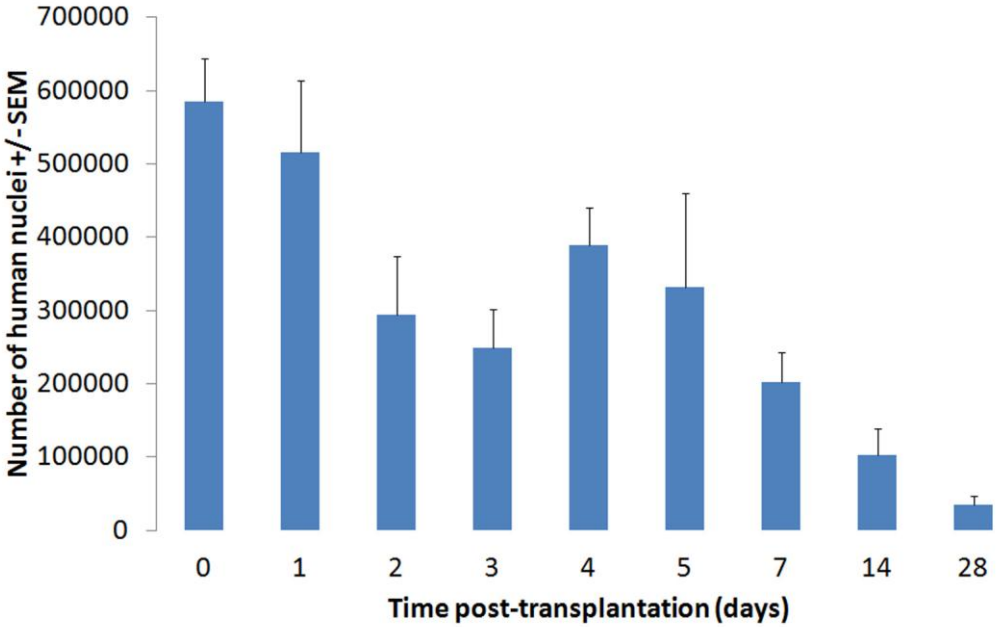

576

577

578 Figure 3

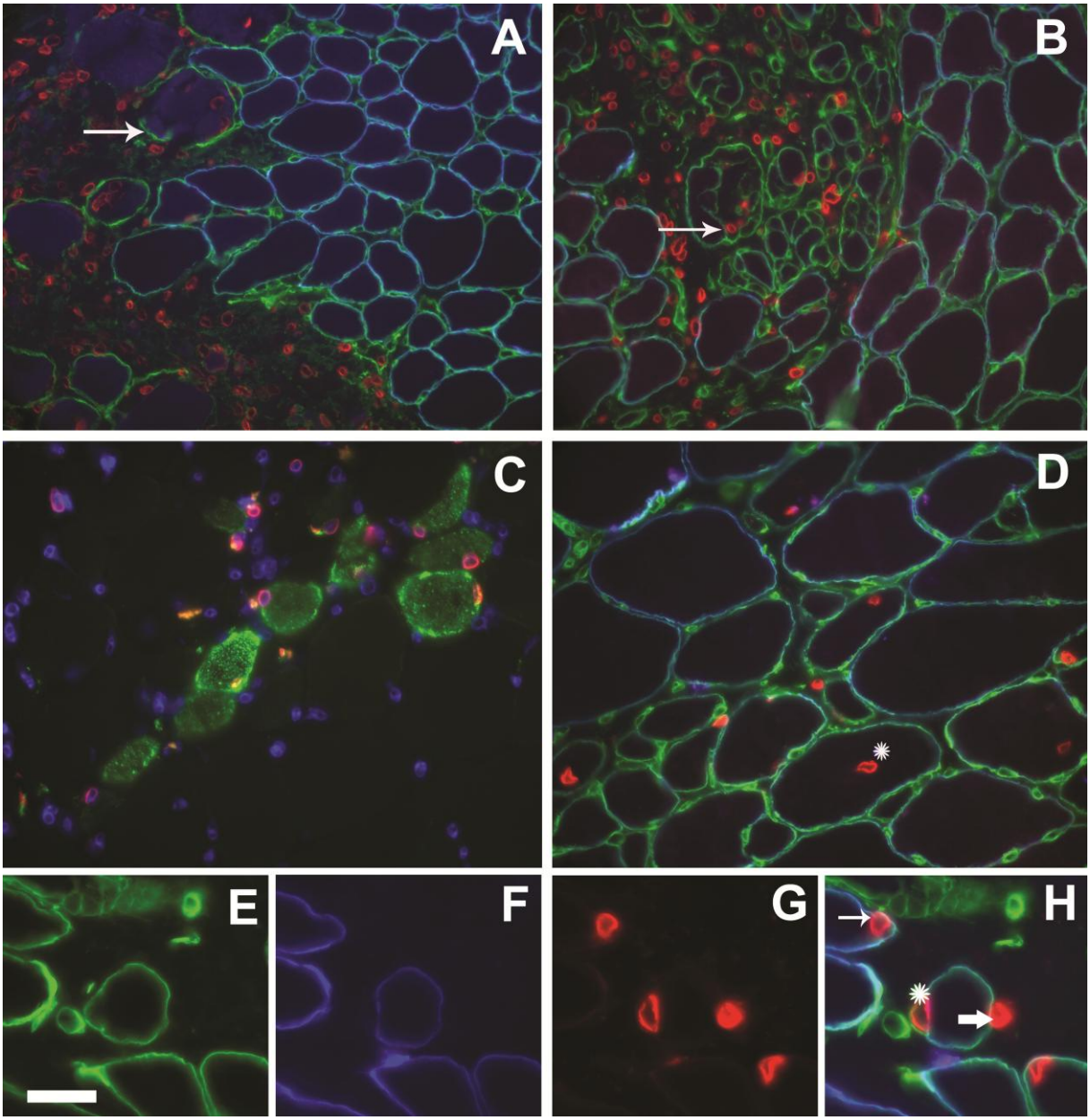

579

580

581 Figure 4

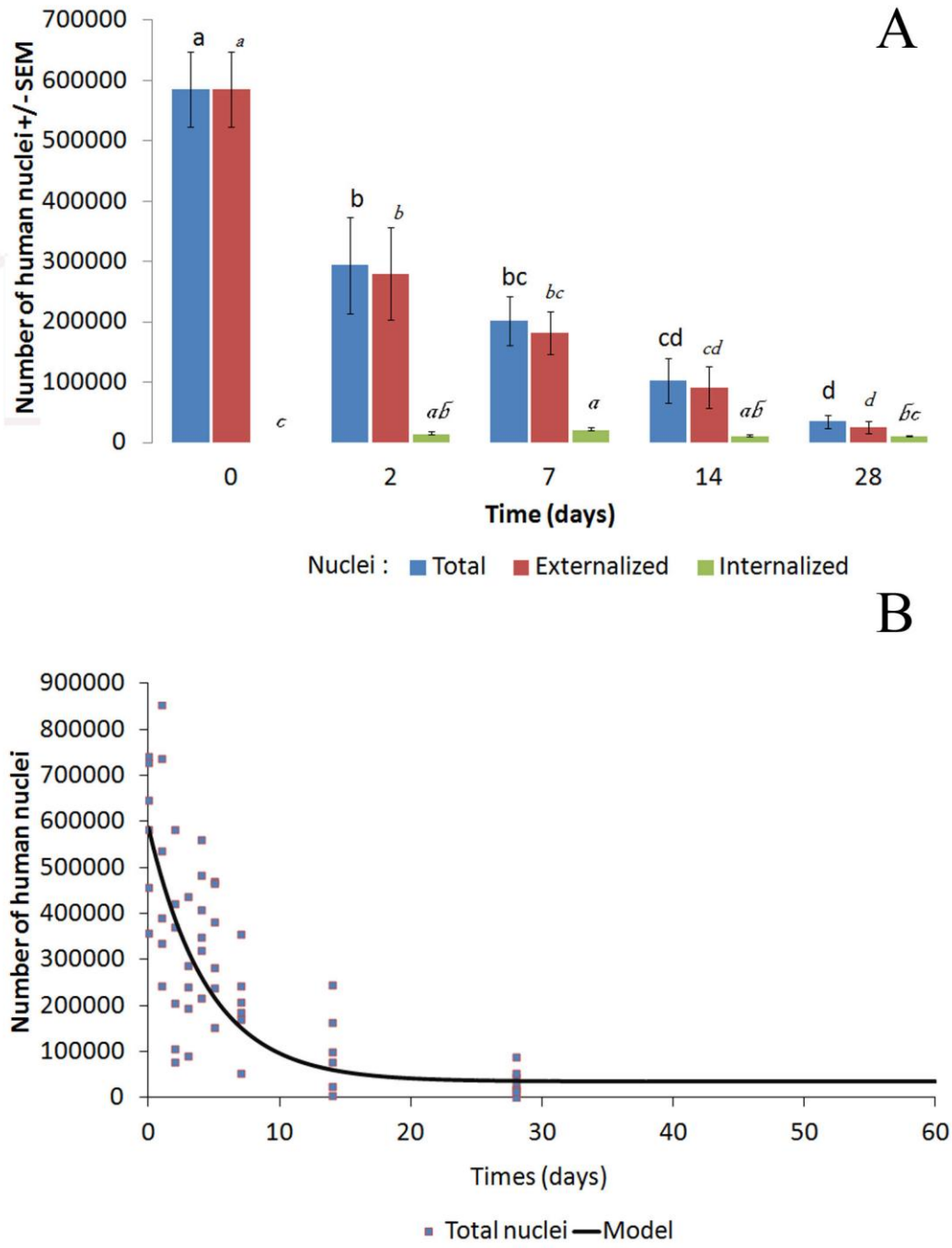

582